

Article

Low-Temperature Plasma Nitriding of 3Cr13 Steel Accelerated by Rare-Earth Block

Yuan You ^{1,2,3,*}, Rui Li ¹ , Mufu Yan ², Jihong Yan ³, Hongtao Chen ⁴, Chaohui Wang ¹, Dongjing Liu ¹, Lin Hong ¹ and Tingjie Han ¹

¹ School of Materials Science and Engineering, Qiqihar University, Qiqihar 161006, China; ly731374908@163.com (R.L.); wch800209@126.com (C.W.); lovccat@163.com (D.L.); hl25802021@163.com (L.H.); htj202021@163.com (T.H.)

² National Key Laboratory of Metal Precision Thermal Processing, School of Materials Science and Engineering, Harbin Institute of Technology, Harbin 150001, China; yanmufu@hit.edu.cn

³ School of Mechanical and Electrical Engineering, Harbin Institute of Technology, Harbin 150001, China; jyan@hit.edu.cn

⁴ School of Materials Science and Engineering, Harbin University of Science and Technology, Harbin 150040, China; htchen83@163.com

* Correspondence: youyuan@qqhru.edu.cn

Abstract: The plasma nitriding of 3Cr13 steel occurred at 450 °C for 4, 8 and 12 h in NH₃ with and without rare earth (RE). The nitrided layers were characterized using an OM, SEM, TEM, XRD, XPS, microhardness tester and electrochemical workstation. The modified layer, with and without La, are composed of a compound layer and diffusion layer from surface to core. After the addition of La during nitriding, the maximum increase of layer thickness, mass gain and average microhardness was 15.6%, 35.8% and 212.50HV_{0.05}, respectively. With the increase of the proportion of ε-Fe₂₋₃N, the passivation zone of the corrosion resistance curve increases from 2.436 to 3.969 V, the corrosion current density decreases, the corrosion potential and pitting potential both increase, and, consequently, the corrosion resistance is significantly improved. Most of the surface microstructures of the nitrided layer was refined by the addition of La. The presence of La reduces the N content in the modified layer, which accelerates the diffusion of N atoms and, thus, accelerates the nitriding process.

Keywords: 3Cr13 steel; plasma nitriding; microstructure; microhardness; corrosion resistance



Citation: You, Y.; Li, R.; Yan, M.; Yan, J.; Chen, H.; Wang, C.; Liu, D.; Hong, L.; Han, T. Low-Temperature Plasma Nitriding of 3Cr13 Steel Accelerated by Rare-Earth Block. *Coatings* **2021**, *11*, 1050. <https://doi.org/10.3390/coatings11091050>

Academic Editor: Alexander D. Modestov

Received: 29 July 2021

Accepted: 28 August 2021

Published: 31 August 2021

Publisher's Note: MDPI stays neutral with regard to jurisdictional claims in published maps and institutional affiliations.



Copyright: © 2021 by the authors. Licensee MDPI, Basel, Switzerland. This article is an open access article distributed under the terms and conditions of the Creative Commons Attribution (CC BY) license (<https://creativecommons.org/licenses/by/4.0/>).

1. Introduction

Because of its low price, it is suitable for a stainless steel working environment with general requirements. Because of its impact resistance, processing formability and high plasticity, it is widely used to manufacture ice blades, scalpels, piston rods, turbine blades and valve parts [1,2]. It can be used for surgical cutting tools, tool materials and structural materials in the fields of medical instruments, the plastics industry and mechanical construction [3]. Compared with other stainless steels, 3Cr13 steel has enhanced toughness and reduced hardness, with relatively worse rust resistance. In order to improve its service life and expand its application, researchers have investigated techniques such as salt bath nitriding [4], cathode cage nitriding [5], radio frequency magnetron sputtering nitriding [6], active screen plasma nitriding [7] and pulse DC plasma nitriding [8] technology processing.

From an economic point of view, it not only reduces the cost, but also improves the surface properties of various steels in an environmentally friendly way. As an efficient and energy-saving thermochemical surface processing and modification technology, it has the advantages of a short processing time, low temperature, reduced brittleness of the nitriding layer, a reduction of work piece deformation and surface flexibility and toughness [9].

China possesses the world's largest reserve of RE elements, which play an important role in the metallurgical industry, military, petrochemical, glass, ceramics, new materials

and agriculture. RE elements are mainly used in tanks, aircraft, lighting sources, polishes and exhaust purification catalysts [10].

In recent years, scientists have explored the impacts of adding RE elements to steel in terms of corrosion resistance [11], strengthening effect [12], contact fatigue limit, bending fatigue limit [13] and other mechanical properties of steel [14,15]. The effects of RE types (cast lanthanum La, pure La block, La_2O_3 , Er_2O_3 , Yb_2O_3 , CeO_2) on the strength, corrosion resistance and fatigue life of steel were also studied. Zhang [16] et al. proved that La reduced the N content in the nitrated layer and promoted the diffusion of interstitial nitrogen from the surface to the interior of the workpiece. La atoms can also attract each other with N atoms in order to achieve the ability of denitrification.

However, there are few studies on plasma nitriding of 3Cr13 stainless steel with the addition of RE. Therefore, it is necessary to conduct a detailed analysis of the properties of 3Cr13 stainless steel with and without the addition of RE. In this paper, 3Cr13 steel has been plasma nitrated at 450 °C for 4, 8 and 12 h in NH_3 , with and without RE. The effects of RE (La) on the microstructure, phase composition, microhardness and corrosion resistance of the modified layer were studied.

2. Materials and Methods

The material used in the present work is 3Cr13 steel with the following chemical composition (wt.%): 0.33C, 12.6Cr, 0.1Ni, 0.48Si, 0.52P, 0.01S and balance Fe. Before nitriding, the steel was solution treated in the box electric furnace SXL-1400C (Shanghai Jvjing Precision Instrument Manufacturing Co., Ltd., Shanghai, China) at 960 °C for 1 h and then quenched in oil. The surface of the sample was polished with water sandpaper (#120 and #240), and then cleaned with alcohol by ultrasonication.

Before using the LDMC-30AFZ plasma nitriding furnace (Wuhan Shoufa Surface Engineering Co., Ltd., Wuhan, China) for the plasma nitriding treatment, the chamber was evacuated to below 10 Pa by a rotary pump. The RE used in the experiment came from the RE block with a volume of $(0.5 \times 0.5 \times 1) \text{ cm}^3$, namely RE0.25. The samples were uniformly tied to the sample frame with iron wire, and the RE block was tied to the center of the sample frame. The nitriding conditions are the same with or without RE. The nitriding experiment was conducted in ammonia (NH_3) with a flux of 100 mL/min at a temperature of 450 °C for 4, 8 and 12 h, and the voltage and working current during nitriding were 260 Pa and 12 A, respectively. After plasma nitriding, the specimens were cooled down slowly inside the vacuum furnace.

The weight gain during the experimental process was obtained using CPA-225D electronic balance (Sai Dolis scientific instruments Beijing Co., Ltd, Beijing, China) with an accuracy of 0.00001 g. A metallographic samples inlaying machine (XQ-1, Shanghai Metallurgical Equipment Company Ltd., Shanghai, China) was used for cross-section sample preparation. The models of grinding water sandpaper were 120#, 240#, 400#, 600#, 800#, 1000#, 1200#, 1500# and 2000#, respectively. The polished samples were etched using a marble solution (2 g $\text{CuSO}_4 + 10 \text{ mL HCl} + 50 \text{ mL H}_2\text{O}$) for 1 s. The cross-section micrographs were observed using an optical microscope (OM, 9XB-PC, Shanghai Optical Instrument No.1 Factory, Shanghai, China). Microhardness was measured with a microhardness tester (HV-1000IS, Shanghai Jvjing Precision Instrument Manufacturing Co., Ltd., Shanghai, China) under an indentation load of 50 g for 15 s. The anodic polarization tests were employed to estimate the corrosion resistance of the specimens in a 3.5 wt.% NaCl solution, the reference electrode was Ag/AgCl and a platinum column was used as the auxiliary electrode. The anodic polarization curves of the specimens were recorded at a sweeping speed of 0.01 V/s. X-ray diffraction (XRD) with Cu-K α radiation ($\lambda = 0.15418 \text{ nm}$) was carried out in the range of angles 20°–100° at 45 kV and 200 mA with a 5° interval step mode using a D8 Advance diffractometer (Bruker, Billerica, MA, USA). The cross-section morphologies of the modified surfaces and the changes in element content with depth were analyzed using a S-3400 scanning electron microscope (SEM, Hitachi, Tokyo, Japan), coupled with energy dispersive X-ray analyzer (EDS) facilities. XPS

analysis was performed in an ultra-high vacuum using a Escalab250XI (Thermo Fisher Scientific, Waltham, MA, USA). The excitation source was monochromatic Al K α radiation, operated at 15 kV and the emission current was 10 mA. The binding energy of C1s neutral carbon peak at 284.6 eV was taken as the reference value and the measured binding energy was modified. The argon ion spray gun (kinetic energy of 3 keV) was used to complete the 30 min incident argon ion sputtering process on the samples in the preparation chamber to ensure that the surface of the samples, at a depth of 100 nm, was clean. The microstructure and grain size of the amorphous samples were observed using a transmission electron microscopy (TEM, JEOL Ltd., Tokyo, Japan) at the operating voltage of 300 kV.

3. Results and Discussion

3.1. Cross-Sectional Microstructure and Depth Analysis

Figure 1a,b are cross-sectional micrographs of 3Cr13 steel after plasma nitriding for 4, 8 and 12 h without and with RE. The nitrided layer is composed of a compound layer and diffusion layer from surface to core. There are distinct boundaries between the compound layer, the diffusion layer and the substrate. The total thickness of the nitrided layer can be obtained according to the microhardness diagrams, the thickness of the compound layer can be obtained according to the ruler in Figure 1, and the difference value is the thickness of the diffusion layer. With the addition of RE, the thickness of the nitrided layer increases with time, and the total thickness of the nitrided layer is 130.4, 161.5 and 185.6 μm , respectively, which is 8.6%, 15.6% and 14.7% higher than that without RE, respectively.

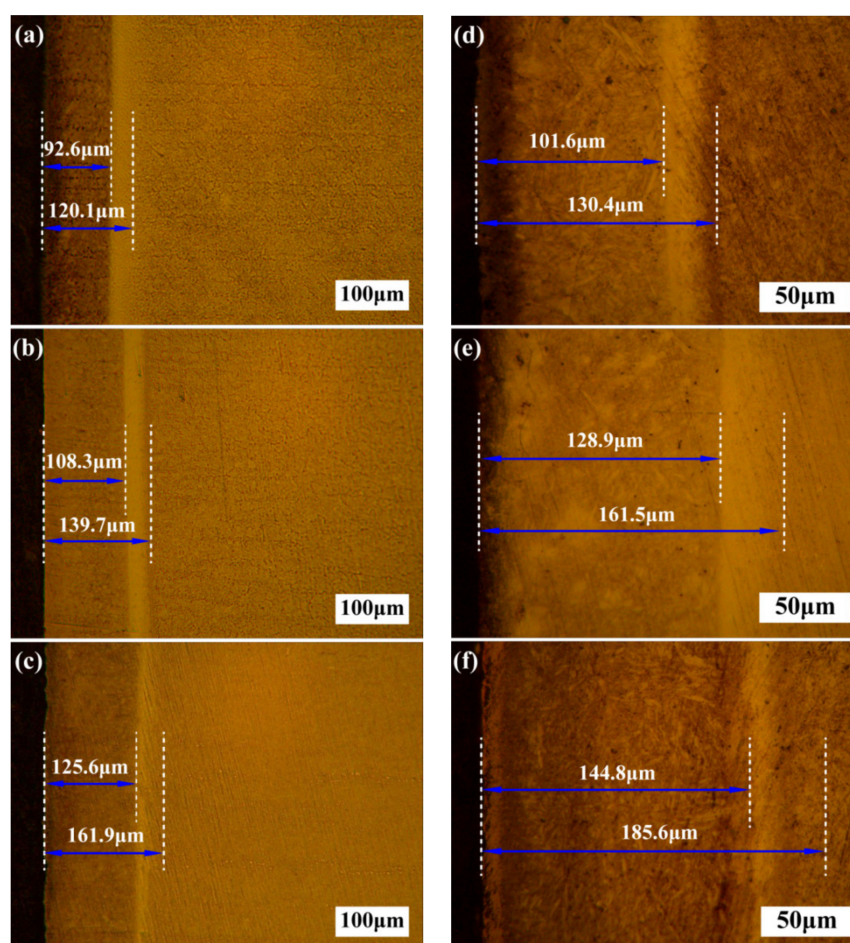


Figure 1. Cross-section micrograph of modified layer of 3Cr13 steel after plasma nitriding (a) h4, (b) h8, (c) h12 without RE and (d) h4, (e) h8, (f) h12 with RE.

Figure 2a,b are histograms of the thickness increase of the modified layer section of 3Cr13 steel after plasma nitriding for 4, 8 and 12 h without and with RE. The change in the thickness of the nitrided layer can be seen more intuitively.

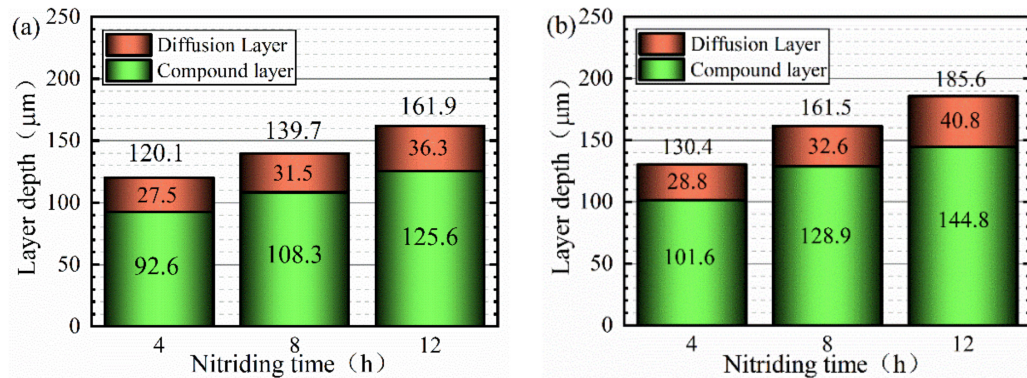


Figure 2. Thickness of modified layer section of 3Cr13 steel after plasma nitriding at different times (a) Without RE (b) With RE.

Figure 3a,b are histograms of the weight gain of 3Cr13 steel after plasma nitriding for 4, 8 and 12 h without and with RE. The weight gain of the sample becomes more significant with the extension of time. With the addition of RE, the weight gain of the nitrided layer is very obvious, reaching 2.31, 3.56 and 4.23 mg/cm², respectively, which is 102.6%, 135.8% and 121.5% higher than that without the addition of RE, respectively.

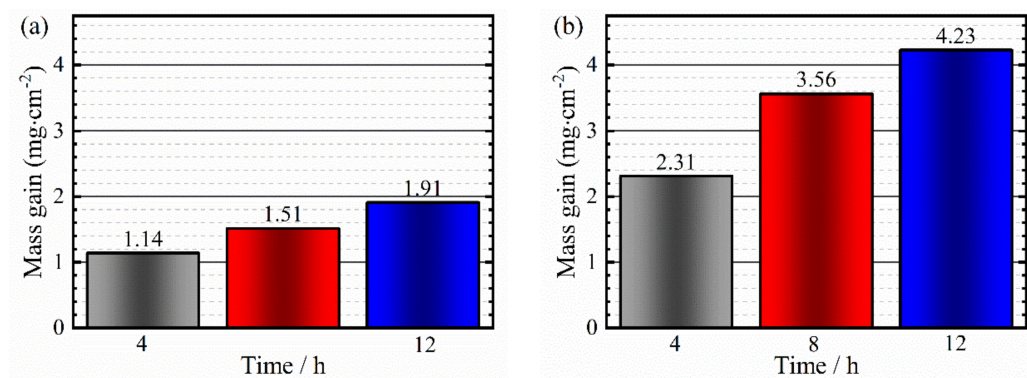


Figure 3. Mass increase per unit area of 3Cr13 steel after plasma nitriding at different times (a) Without RE (b) With RE.

3.2. Microhardness Profile

Figure 4a,b are the microhardness diagrams of 3Cr13 steel after plasma nitriding for 4, 8 and 12 h without and with RE. Microhardness varies with the nitriding time and depth of the nitriding layer. From the surface layer to the dense compound layer, the microhardness first increases (gradual horizontal hardening), reaches the peak and then gradually decreases. A platform appears (flat horizontal hardening) when it reaches the diffusion layer. There is a sudden drop from the diffusion layer to the substrate boundary and then a gradual transition to the substrate. After 4, 8 and 12 h of nitriding, the average hardness of the modified layer is 813.53HV_{0.05}. After 4, 8 and 12 h of RE nitriding, the average hardness of the modified layer is 1026.03HV_{0.05}, which demonstrates an increase of 212.50HV_{0.05} compared to the sample without RE. The increase in surface hardness was directly related to the formation of fine and uniform ε-Fe₂₋₃N and γ'-Fe₄N nitride phases in the cemented layer, as shown in Figure 5. The comparison between the microhardness and the depth profile of nitrogen concentration indicated that this was related to the diffusion of N. The N content on the surface (0 μm) reaches the maximum and the surface hardness reaches the maximum. From the compound layer to the diffusion layer and until the substrate, the surface hardness decreased significantly with the decrease of N content.

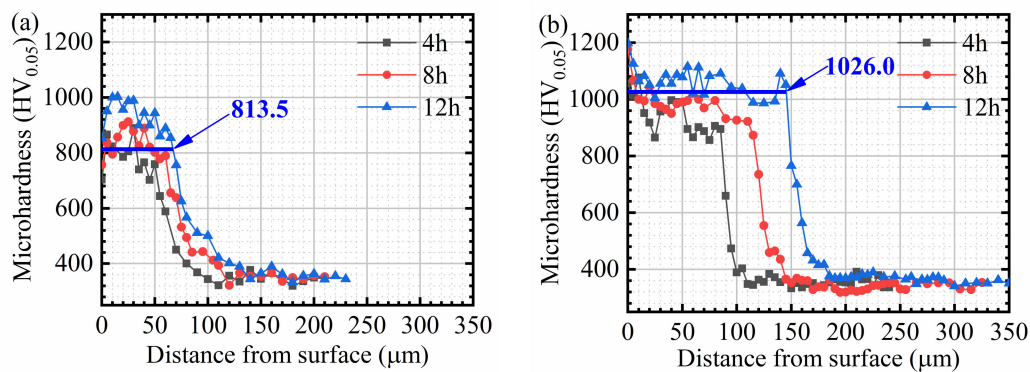


Figure 4. The microhardness diagrams of 3Cr13 steel after plasma nitriding at different times (a) Without RE (b) With RE.

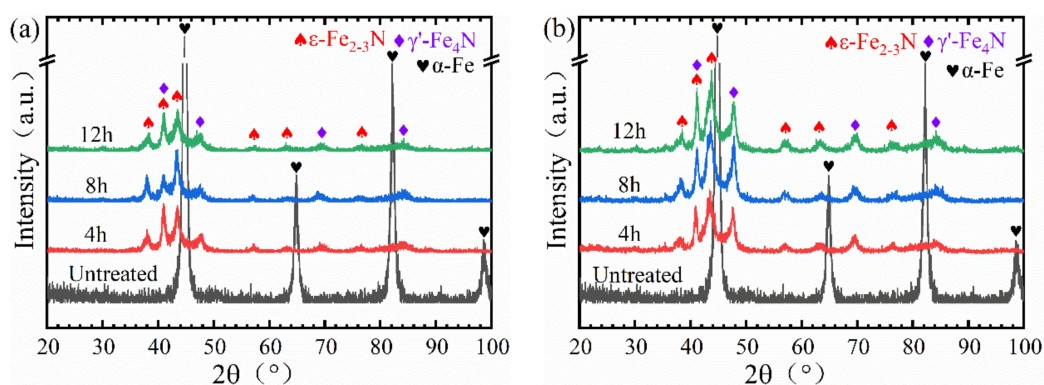


Figure 5. XRD pattern of the modified layer of 3Cr13 steel after plasma nitriding at different times (a) Without RE (b) With RE.

3.3. XRD

Figure 5a,b are the XRD pattern of the modified layer of 3Cr13 steel after plasma nitriding for 4, 8 and 12 h without and with RE. In Figure 5a, the main phase is ϵ -Fe_{2.3}N, the secondary phase is γ' -Fe₄N. After the addition of La, the intensity of the ϵ -Fe_{2.3}N diffraction peak is significantly enhanced, and the content of ϵ -Fe_{2.3}N in the modified layer is greatly increased. Reference [14] shows that ϵ -Fe_{2.3}N improved the corrosion resistance to a significant extent, and more than that of γ' -Fe₄N. At the same time, due to the La atoms dissolving into the nitride layer, the lattice distortion results in increased microhardness [12].

3.4. Polarization Curve and Fitting Data Analysis

Figure 6a,b display the corrosion resistance curve of 3Cr13 steel after plasma nitriding for 4, 8 and 12 h without and with RE. With or without the addition of RE, the passivation zone of the corrosion resistance curve becomes wider with the increase of time, the corrosion resistance is slightly enhanced.

The data relating to the corrosion rate, corrosion potential (E_0), polarization resistance (R_p) and corrosion current (I_0) on the surface of the modified layer are shown in Tables 1 and 2. In comparing the samples with and without RE nitriding, with the increase of time, the corrosion rate of the modified layer decreased slightly, and the corrosion resistance of the modified layer increased slightly. It can be concluded that the modified layer has the best corrosion resistance after 12 h of RE nitriding, with the corrosion rate decreasing to 0.9255×10^{-2} mm/a.

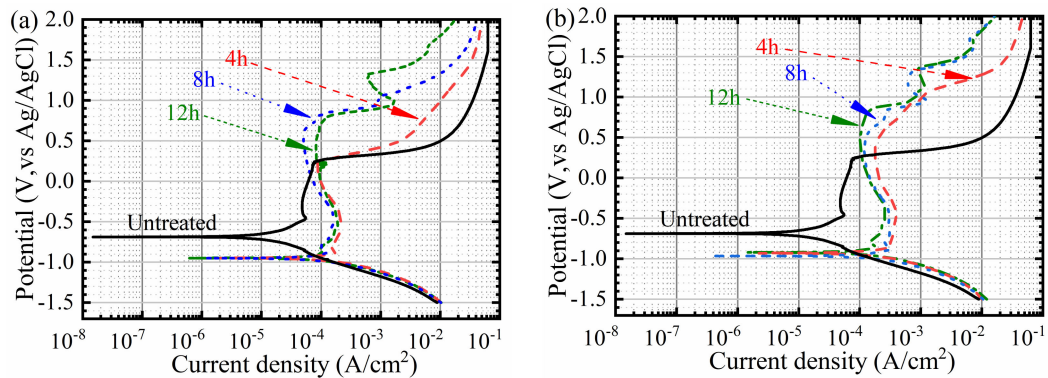


Figure 6. Corrosion resistance curve of modified layer of 3Cr13 steel after plasma nitriding at different times (a) Without RE (b) With RE.

Table 1. Fitting data of the polarization curve of the modified layer of 3Cr13 steel after plasma nitriding at different times.

Time/h	Corrosion Rate/($\times 10^{-2}$ mm·a $^{-1}$)	Rp/($\times 10^{-3}$ Ω ·cm $^{-2}$)	I ₀ /($\times 10^{-5}$ A·cm $^{-2}$)	E ₀ /V	Passivation Zone/V
Untreated	49.746	61.681	4.22930	−0.87501	1.038
4	1.3519	2.2697	1.14930	−0.94865	1.352
8	1.2851	2.3995	1.04978	−0.94805	1.801
12	1.0895	2.7796	1.00630	−0.95095	2.436

Table 2. Fitting data of the polarization curve of the modified layer of 3Cr13 steel after RE plasma nitriding at different times.

Time/h	Corrosion Rate/($\times 10^{-2}$ mm·a $^{-1}$)	Rp/($\times 10^{-3}$ Ω ·cm $^{-2}$)	I ₀ /($\times 10^{-5}$ A·cm $^{-2}$)	E ₀ /V	Passivation Zone/V
Untreated	49.746	61.681	4.22930	−0.87501	1.038
4	1.2288	2.3767	0.89491	−0.91983	2.105
8	1.0463	2.4935	0.73978	−0.94882	2.401
12	0.9255	2.9950	0.63733	−0.92949	2.563

The enhanced corrosion resistance is due to the presence of a dense nitride-rich layer on the ϵ -nitride surface, as more nitride helps protect the surface from corrosion [17]. Figure 5 proved that the formation of ϵ -Fe₂₋₃N and γ' -Fe₄N greatly improves the corrosion resistance of the modified layer [18].

3.5. SEM

The C, N, Cr, Fe and La elements at different locations of the modified layer were measured by point scanning. The content of N element decreases gradually from the surface to the substrate, while the content of Fe element increases gradually.

As shown in Figure 7a, as the depth of the nitriding layer increases, Fe content gradually decreases, N content reaches as high as 4.57 at.%, and then continues to decline to 0.23 at.%. As shown in Figure 7b, as the depth of the nitriding layer increases, Fe content gradually decreases, the N content in the surface layer does not reach the maximum, but gradually increased to a maximum of 2.72%, and then gradually transitioned to the substrate.

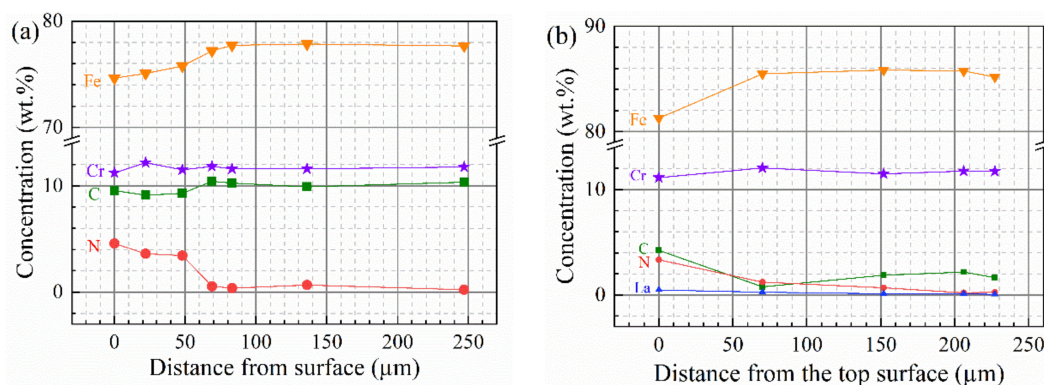


Figure 7. Element content depth distribution of the modified layer of 3Cr13 steel after plasma nitriding for 12 h (a) Without RE (b) With RE.

First, ion bombardment produces La ions and some neutral ions, which are deposited on the surface of stainless steel and play a role in cleaning and activation, increasing the concentration of surface nitrogen [9]. Then, due to the large size difference between La and Fe atoms, La causes obvious distortion in the surrounding lattice. Meanwhile, La enhances the surface bombardment effect, increasing the crystal defects such as vacancies and dislocations and further reducing the N content in the nitrided layer, which accelerates the diffusion of N atoms and produces solid solution strengthening. Thus, the thickness of compound and effective hardening layer is increased, and the nitriding process is accelerated [19,20].

Figure 8a,b are the element depth profile of the modified layer of 3Cr13 steel after plasma nitriding for 12 h, without and with RE. The percentage of La, C and N are measured by linear scanning. As can be seen from Figure 8a,b, the Cr content of both C-layer (0–125.6 μm) and D-layer (0–144.8 μm) increased, while the N content decreased significantly. As shown in Figure 9a, the total diffusion depth increased from 145.3 to 157.9 μm , the contents of Cr and N decreased in the D-layer layer (125.6–145.3 μm), while the contents of Cr and N basically remained unchanged in the D-layer (144.8–157.9 μm) layer in Figure 9b. The La content decreased gradually. The addition of La greatly promoted the diffusion of N and reduced the precipitation of CrN.

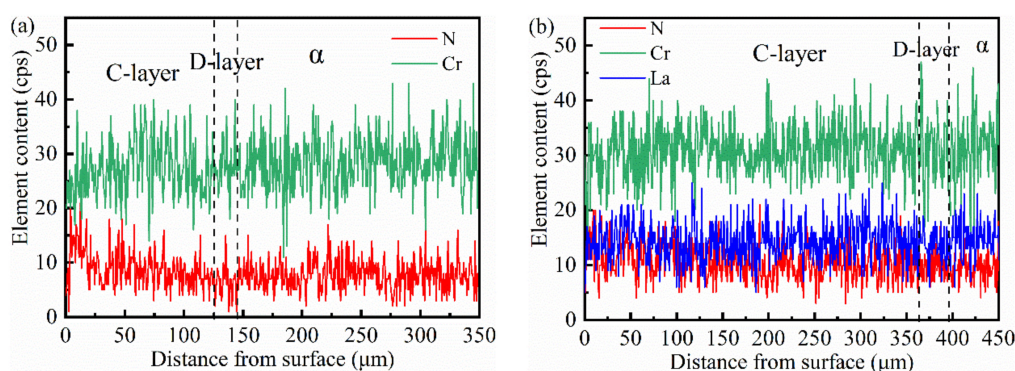


Figure 8. Element depth profile of modified layer of 3Cr13 steel after plasma nitriding for 12 h (a) Without RE (b) With RE.

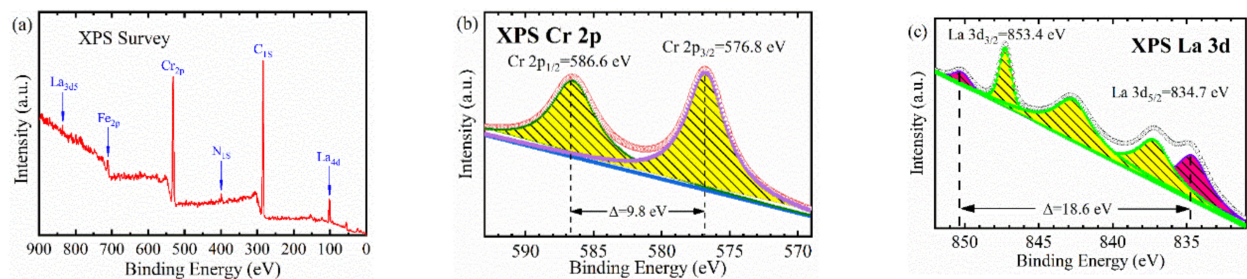


Figure 9. XPS spectra modified layer of 3Cr13 steel after RE plasma nitriding for 12 h (a) Survey spectra (b) Cr 2p spectra (c) La3d spectra.

3.6. XPS

The detailed chemical characteristics of various elements in the surface layer are analyzed by XPS characterization in order to obtain information about the formation of surface nitride in the plasma ionitriding process. The results are shown in Figure 9a.

In order to determine the possibility of producing a Cr-N bond on the sample surface under consideration and to study the content of CrN on the surface, the XPS spectrum of a high-resolution Cr2P is shown in Figure 9b. A strong peak (a weak peak) was observed in the XPS spectrum of Cr2P, with a peak position matching the orbital 2P1/2 (586.6 eV) and orbital 2P2/3(576.8 eV) [21].

Figure 9c shows the photoemission spectra of La 3D rays obtained by surface modification with monochromatic Al Ka photons. The main peak of the La3d XPS spectrum was about 853.4 and 834.7 eV, belonging to La3d3/2 and La3d5/2, respectively [22]. The results show that the successful diffusion of the La element to the nitride surface can not only spread to a significant depth of the surface, but can also help the gap nitrogen to diffuse to a deeper layer of the workpiece, and improve the structure and properties of the modified layer.

3.7. TEM

Figure 10a,b show typical transmission electron microscope images and diffraction ring images of nanocrystallization of 3Cr13 steel at 10 μm from the sample surface after RE nitriding for 12 h. According to the scale and the comparison of the standard XRD diffraction peak pattern in Figure 10b, the inner ring corresponds to the crystal plane γ' -Fe₄N (311), and the outer ring corresponds to the crystal plane ϵ -Fe₃N (112). The SAED patterns shows that there are a large number of γ' -Fe₄N and ϵ -Fe₃N particles. The addition of La can further refine the grain size of the nanocrystalline layer [23], and the results indicate that the addition of La can produce a microalloying effect on the nitride layer of 3Cr13 steel.

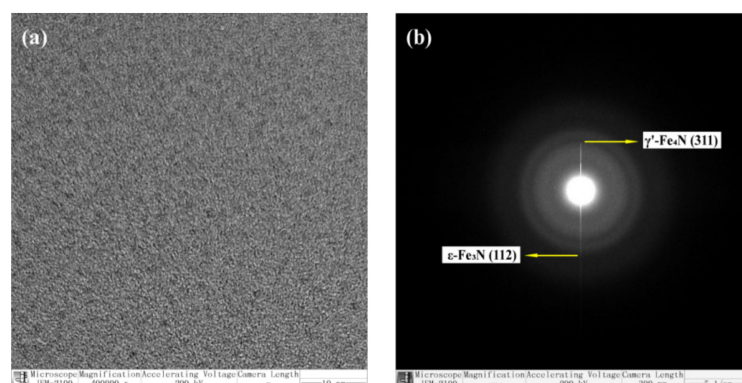


Figure 10. TEM bright field image (a) and corresponding SAED pattern (b) of surface nanometer layer of modified 3Cr13 steel after RE plasma nitriding for 12 h.

4. Conclusions

In this paper, 3Cr13 steel was plasma nitrided for 4, 8 and 12 h at 450°C in NH₃ atmosphere with and without RE, and the following conclusions were drawn:

1. The nitrided layer was composed of a compound layer and diffusion layer from surface to core. The total thickness of the RE nitrided layer increased by 8.6%, 15.6% and 14.7% more than that of the layer without RE. The thickness of the compound layer was increased by 9.7%, 19.0% and 15.3% more than that of the compound layer without RE. The mass gain of the RE nitrided layer was significant, and increased by 36% more than that of plain nitriding.
2. The modified layer was mainly composed of ϵ -Fe₂₋₃N and γ' -Fe₄N nitride phases. The addition of RE (La) increased the phase ratio of ϵ -Fe₂₋₃N in the surface layer. The corrosion current density was decreased, the corrosion resistance was increased, and the passivation zone gradually widened. The addition of RE (La) made the passivation more obvious, thus improving the corrosion resistance.
3. The average hardness of the compound layer was 813.53HV_{0.05}. The average hardness of the RE compound layer was 1026.03HV_{0.05}, which increased by 212.50HV_{0.05}.
4. SEM (EDS) and XPS demonstrated the presence of La, and the N content gradually decreased with the depth of the nitride layer. La diffused into the interior of the layers and further reduced the N content in the nitride layer, which accelerated the diffusion of N atoms and thus promoted the nitriding process.
5. There are many γ' -Fe₄N and ϵ -Fe₃N particles in the nitrided layer. The addition of RE further refined the microstructure in the nitrided layer, in which the microalloying effect was produced to strengthen the modified layer.

Author Contributions: Investigation, R.L. and Y.Y.; Writing—Review and Editing, R.L., Y.Y., M.Y., J.Y., H.C., C.W., D.L., L.H. and T.H. All authors have read and agreed to the published version of the manuscript.

Funding: Supported by the National Natural Science Foundation of China (51401113) and Natural Science Foundation of Heilongjiang Province of China (E2016069), Heilongjiang Postdoctoral Financial Assistance (LBH-Z16061), the Fundamental Research Funds in Heilongjiang Provincial Universities (135309504).

Institutional Review Board Statement: Not applicable.

Informed Consent Statement: Not applicable.

Data Availability Statement: Data is contained within the article.

Conflicts of Interest: The authors declare no conflict of interest.

References

1. Xi, Y.T.; Liu, D.X.; Han, D. Improvement of corrosion and wear resistances of AISI 420 martensitic stainless steel using plasma nitriding at low temperature. *Surf. Coat. Technol.* **2008**, *202*, 2577–2583. [[CrossRef](#)]
2. Pinedo, C.E.; Monteiro, W.A. On the kinetics of plasma nitriding a martensitic stainless steel type AISI 420. *Surf. Coat. Technol.* **2004**, *179*, 119–123. [[CrossRef](#)]
3. Çetin, A.; Tek, Z.; Öztarhan, A.; Artunc, N. A comparative study of single and duplex treatment of martensitic AISI 420 stainless steel using plasma nitriding and plasma nitriding-plus-nitrogen ion implantation techniques. *Surf. Coat. Technol.* **2007**, *2019*, 8127–8130. [[CrossRef](#)]
4. Luo, G.; Zheng, Z.; Ning, L.; Tan, Z.; Tong, J.; Liu, E. Failure analysis of AISI 316L ball valves by salt bath nitriding. *Eng. Fail. Anal.* **2020**, *111*, 104455. [[CrossRef](#)]
5. Shen, H.; Wang, L. Mechanism and properties of plasma nitriding AISI 420 stainless steel at low temperature and anodic (ground) potential. *Surf. Coat. Technol.* **2020**, *403*, 126390. [[CrossRef](#)]
6. Nakasa, K.; Gao, S.; Yamamoto, A.; Sumomogi, T. Plasma nitriding of cone-shaped protrusions formed by sputter etching of AISI 420 stainless steel and their application to impression punch to form micro-holes on polymer sheets. *Surf. Coat. Technol.* **2019**, *358*, 891–899. [[CrossRef](#)]
7. Li, Y.; He, Y.; Xiu, J.; Wang, W.; Zhu, Y.; Hu, B. Wear and corrosion properties of AISI 420 martensitic stainless steel treated by active screen plasma nitriding. *Surf. Coat. Technol.* **2017**, *329*, 184–192. [[CrossRef](#)]

8. Corengia, P.; Ybarra, G.; Moina, C.; Cabo, A.; Broitman, E. Microstructural and topographical studies of DC-pulsed plasma nitrided AISI 4140 low-alloy steel. *Surf. Coat. Technol.* **2005**, *200*, 2391–2397. [[CrossRef](#)]
9. Wu, K.; Liu, G.Q.; Wang, L.; Xu, B.F. Research on new rapid and deep plasma nitriding techniques of AISI 420 martensitic stainless steel. *Vacuum* **2010**, *84*, 870–875. [[CrossRef](#)]
10. Cleugh, D.; Blawert, C.; Steinbach, J.; Ferkel, H.; Mordike, B.L.; Bell, T. Effects of rare earth additions on nitriding of EN40B by plasma immersion ion implantation. *Surf. Coat. Technol.* **2001**, *142–144*, 392–396. [[CrossRef](#)]
11. Medina, A.; Aguilar, C.; Béjar, L.; Oseguera, J.; Ruíz, A.; Huape, E. Effects of post-discharge nitriding on the structural and corrosion properties of 4140 alloyed steel. *Surf. Coat. Technol.* **2019**, *366*, 248–254. [[CrossRef](#)]
12. Dai, M.; Li, C.; Hu, J. The enhancement effect and kinetics of rare earth assisted salt bath nitriding. *J. Am. Ceram. Soc.* **2016**, *688*, 350–356. [[CrossRef](#)]
13. Cheng, X.-H.; Xie, C.-Y. Effect of rare earth elements on the erosion resistance of nitrided 40Cr steel. *Wear* **2003**, *254*, 415–420. [[CrossRef](#)]
14. Tang, L.N.; Yan, M.F. Effects of rare earths addition on the microstructure, wear and corrosion resistances of plasma nitrided 30CrMnSiA steel. *Surf. Coat. Technol.* **2012**, *206*, 2363–2370. [[CrossRef](#)]
15. Chen, X.; Xiangyun, B.; Xiao, Y.; Chengsong, Z.; Tang, L.; Cui, G.; Yang, Y. Low-temperature gas nitriding of AISI 4140 steel accelerated by LaFeO₃ perovskite oxide. *Appl. Surf. Sci.* **2019**, *466*, 989–999. [[CrossRef](#)]
16. Zhang, C.S.; Yan, M.F.; Sun, Z. Experimental and theoretical study on interaction between lanthanum and nitrogen during plasma rare earth nitriding. *Appl. Surf. Sci.* **2013**, *287*, 381–388. [[CrossRef](#)]
17. Liu, R.L.; Yan, M.F.; Wu, D.L. Microstructure and mechanical properties of 17-4PH steel plasma nitrocarburized with and without rare earths addition. *J. Mater. Res.* **2010**, *210*, 784–790. [[CrossRef](#)]
18. Liu, R.L.; Qiao, Y.J.; Yan, M.F.; Fu, Y.D. Layer growth kinetics and wear resistance of martensitic precipitation hardening stainless steel plasma nitrocarburized at 460A degrees C with rare earth addition. *Met. Mater. Int.* **2013**, *19*, 1151–1157. [[CrossRef](#)]
19. You, Y.; Yan, J.H.; Yan, M.F. Atomistic diffusion mechanism of rare earth carburizing/nitriding on iron-based alloy. *Appl. Surf. Sci.* **2019**, *484*, 710–715. [[CrossRef](#)]
20. Anjos, A.D.; Scheuer, C.J.; Brunatto, S.F.; Perito Cardoso, R. Low-temperature plasma nitrocarburizing of the AISI 420 martensitic stainless steel. Microstructure and process kinetics. *Surf. Coat. Technol.* **2015**, *275*, 51–57. [[CrossRef](#)]
21. Alphonsa, I.; Chainani, A.; Raole, P.M.; Ganguli, B.; John, P.I. A study of martensitic stainless steel AISI 420 modified using plasma nitriding. *Surf. Coat. Technol.* **2002**, *150*, 263–268. [[CrossRef](#)]
22. Liu, T.K.; Qian, J.N.; Yao, Y.Y.; Shi, Z.; Han, L.; Liang, C.; Li, B.; Dong, L.; Fan, M.; Zhang, L. Research on SCR of NO with CO over the Cu_{0.1}La_{0.1}Ce_{0.8}O mixed-oxide catalysts: Effect of the grinding. *Mol. Catal.* **2017**, *430*, 43–53. [[CrossRef](#)]
23. Liu, R.L.; Yan, M.F. Effects of rare earths on nanocrystalline for nitrocarburised layer of stainless steel. *Mater. Struct.* **2017**, *33*, 1346–1351. [[CrossRef](#)]